Numerical simulation tool and experimental set-up for measuring the modal structure of a broad area semiconductor laser diode

Fernando Carlos Romano
Center for Lasers and Applications
IPEN-CNEN/SP
São Paulo, Brazil
fernando.romano@usp.br

Niklaus Ursus Wetter
Center for Lasers and Applications
IPEN-CNEN/SP
São Paulo, Brazil
nuwetter@ipen.br

Abstract— **A computer simulation model for a single stripe, multimode laser diode of the type broad area laser diode (BALD) was built. In sequence, an experimental set-up preparation followed the numeric tool with the objective of identifying the lateral modes by using the frequency beat technique in the RF spectrum. A spectrum analyzer measured the signals emitted by the BALD using the fast Fourier transform (FFT) method.** (*Abstract*)

Keywords— *laser diode, transverse modes, semiconductor laser, multimode laser, laser simulation, BALD (key words)*

I. INTRODUCTION

Single broad area semiconductor lasers denote good beam quality performance under pulsed conditions. Otherwise, when driven by a continuous current, they present beam degradation and filamentation effects. The goal of this work is to provide a Matlab based numerical simulation tool and a testing method for a single stripe semiconductor multimode laser for controlling the transverse electromagnetic modes aiming at designing and testing of laser systems based on BALD semiconductor lasers in continuous mode.

II. SIMULATION MODEL DEVELOPMENT

Our computer model description is based on a set of rate equations adapted from Kubodera's work [1] to a broad area diode laser in stationary condition, $dn/dt = 0$, $ds/dt = 0$, where n means the carrier population inversion density and s stands for the photon density. Calculations for the charge density distribution along the cavity transverse direction and the coupled stimulated intensities of each mode are provided by the numerical tool. Steady state rate equations supply the description of the current distribution density r(x,y,z) and the photon distribution density of the i_{th} transverse mode s_i(x,y,z). Rate equations for carrier density distribution is represented by equation (1), whereas equation (2) corresponds to the produced photons. I_o is the saturation current for lasing and γ_i corresponding to the cavity loss factor. Total decay time τ_f in the second term of equation (2) means the total recombination time of carriers within the active region for all processes [2] according the spontaneous radiative and non-radiative effects and the Auger recombination described by $AN+BN^2+CN^3$, c is the speed of light, L_{ci} is the round trip cavity loss and l is the cavity length. The correspondent carrier flux is calculated according to a Gaussian profile distribution [6] for the waveguide in the transverse x direction with a variable waist size at the center that increases when the pump current

increases, while along the vertical axis y no changes are applicable. S_i is the photon number of the i_{th} mode in the active layer and σ is the laser transition cross-section. Equation (5) describes the necessary threshold current $R_{th,i}$ for an additional lateral mode i in the presence of j other lateral modes already oscillating. For example, in order to evaluate if mode TEM_{10} and TEM_{00} are oscillating simultaneously, we need to solve the two non-linear equations: One investigating if TEM_{10} oscillates in the presence of TEM_{00} and another investigating if TEM_{00} continues to oscillate if TEM_{10} also starts to oscillate. r_o and s_{oi} are the normalized quantities respectively for the charge distribution r(x,y,z) and photon density s_i(x,y,z) of mode i. The threshold level for the i_{th} transverse mode occurrence is represented by R_{th} in equation (5).

$$\frac{dn(x,y,z)}{dt} = r(x,y,z) - \frac{n(x,y,z)}{\tau_f} - c\sigma n(x,y,z)\sum_{i=1}^{m} s_i(x,y,z) \quad (1)$$

$$\frac{dS_i}{dt} = c\sigma \iiint_{cavity} n(x,y,z)s_i(x,y,z)d\vartheta - \gamma_i S_i \quad (2)$$

$$S_i = \iiint S_i(x,y,z)d\vartheta \quad (3)$$

Where:

$$\gamma_i = \frac{cL_{ci}}{2l} \quad (4)$$

$$\frac{I_o\gamma_i}{R_{th,i}} = \iiint \frac{S_{oi}(x.y.z)r_o(x,y,z)}{\frac{S_j s_{oj}(x,y,z)}{I_o}} dv \quad (5)$$

With:

$$I_o = \frac{1}{c\sigma\tau} \quad (6)$$

From the above one calculates that the beam waist at current I_1 with respect to the threshold current [6] I_2 is given by:

$$w(I_1) = \left(\frac{I_1}{I_2}\right)^{1/4} \quad (7)$$

Special plot representations are available from this software tool in order to demonstrate the transverse modes and their spatial distributions with relative widths in the near field region. Fig. 1 depicts a simulation of the TEM_{40} mode for the BALD at a specific pump power while Fig. 2 does so for the TEM_{10}.

Spatial transverse modes are accurately represented by the sourced pumping charge for each specific individual power amount corresponding to each mode index. Fig. 3 denotes

modes TEM_{00} until TEM_{40} with their individual steady-state responses as a function of the pumped diode current.
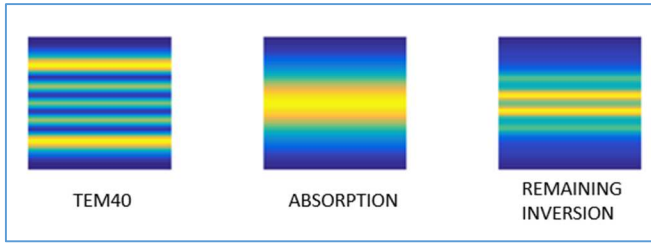

Fig 1. Plot of TEM_{40} mode, initial carrier density inside the active region in x-direction and remaining inversion after TEM_{40} oscillation.

Fig 2. Plot of TEM_{10} mode, initial carrier density inside the active region and remaining inversion after TEM_{10} oscillation.

For this simulation, the following waveguide sizes have been considered:

- Cavity depth = 300 um (x direction);
- Cavity height = 1 um (y direction);
- Cavity length = 4 mm (z direction).

As can be seen in figure 3, threshold values for the modes are approximately evenly spaced for TEM_{00} to TEM_{40} starting with TEM_{00}. Simulation of figure 3 has been done for a waveguide without AR coating and, therefore, threshold values serve only for comparative purposes.
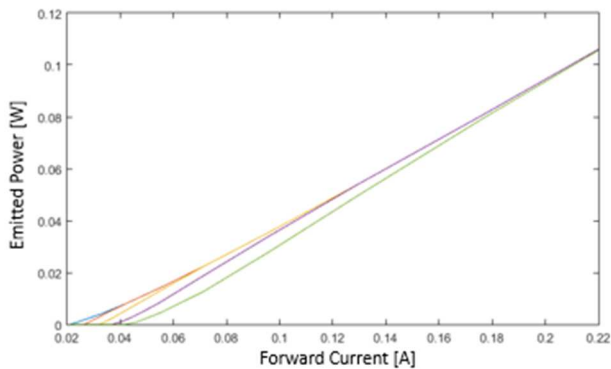

Fig 3. Emitted power of BALD as a function of current for the first oscillating modes. Blue: TEM_{00}; red: TEM_{10}; yellow TEM_{20}; purple: TEM_{30} and green: TEM_{40}. As observed the TEM_{40} threshold is at least twice higher than the TEM_{00} mode.

III. MEASUREMENT METHOD

The demonstration of how two waves with close frequency levels interact each other, and how this phenomenon can give us the opportunity to use a simpler method, in comparison with traditional optical instrumentations, are the objectives of this section. The two waves in reference are depicted in Fig. 4a. In the upper curves, they are combining spatially, and for the bottom, we can see the result as an effect of the two related frequencies beating. The resultant wavelength is much bigger than their predecessors are, and as per analogy, a lower outgoing frequency. In Fig. 4b the low frequency envelope f_2-f_1 is clearly visible. When working with oscillations with a spectrum close to the visible and near infrared radiations, in the range of hundreds of THz, the signal beat frequencies range come down to a few GHz, then becoming their measurement feasible for simpler electronic instruments, as such as an oscilloscope with fast Fourier transformation (FFT) calculation resource.

A. Self-heterodyning process

The process of interference between two waves is conveniently illustrated by Fig. 4a and 4b where we can see the beat notes in terms of spectrum and amplitude. A spectrum analyzer scans the signals emitted by the BALD using a spatially resolved auto heterodyne method. The mathematical basis for the heterodyne process is described below.
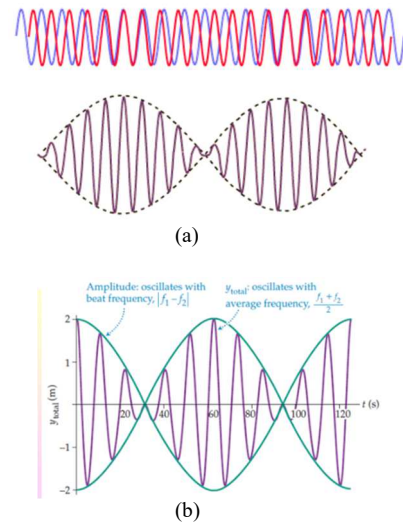

(a)

(b)

Fig 4. a,b. Heterodyne process between two waves of different frequencies, highlighting the resulting spectra and amplitudes.

Let e_1 = sin $(2\pi f_1 t)$ and e_2 = sin $(2\pi f_2 t)$ be two signals with different frequencies using the trigonometric identity of equation (8), the heterodyne synthesis is shown analytically by Fig. 5, and graphically by Fig. 6.

$$sen\theta_1.sen\theta_2 = \frac{1}{2}\cos(\theta_1 - \theta_2) - \frac{1}{2}\cos(\theta_1 + \theta_2) \qquad (8)$$

$$sen(2\pi f_1 t).sen(2\pi f_2 t) = \frac{1}{2}\cos[2\pi(f_1 - f_2)t] - \frac{1}{2}\cos[2\pi(f_1 + f_2)t] \quad (9)$$
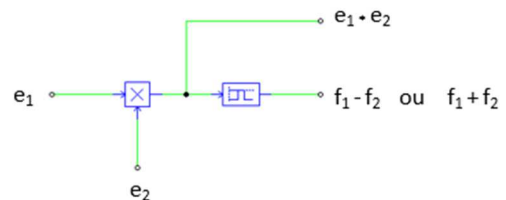

Fig 5. Analytic block representation for a heterodyne process with a two-wave interference in between e_1 and e_2.

With:

$$e_1(t) = [E_1 + e_m(t)].\cos(\omega_1 t) \qquad (10)$$
$$e_2(t) = E_2.\cos(\omega_2 t) \qquad (11)$$

$$e_1.e_2 = \left\{\left[\frac{1}{2}(E_2[E_1 + e_m(t)])\cos(\omega_2 - \omega_1)t\right] + \left[\frac{1}{2}(E_2[E_1 + e_m(t)])\cos(\omega_2 + \omega_1)t\right]\right\} \quad (12)$$

$$= \left\{\left[\frac{1}{2}(E_2[E_1 + e_m(t)])\cos(2\pi(f_2 - f_1))t\right] + \left[\frac{1}{2}(E_2[E_1 + e_m(t)])\cos(2\pi(f_2 + f_1))t\right]\right\} \quad (13)$$
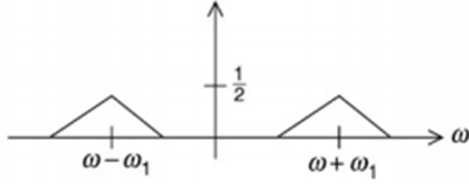

Fig 6. Bilateral spectrum obtained in the heterodyne process (Fourier transform).

The first term of equation (14), corresponding to the term (f_2-f_1), which is the term of interest for the laboratory measurements. For the extraction of the input signal phase, represented by the parameter Θ_1, we have, with the A_1 and A_2 corresponding to the amplitudes of both signals that cross the non-linear element, the convolution process and either getting the frequency of the reference signal identical to the signal input. Fig. 6 represents its graphic convolution. Thus means:

$$A_1\cos(\omega_1 t + \theta_1).A_2\cos(\omega_1 t) = \frac{A_1 A_2}{2}\cos\theta_1 + \frac{A_1 A_2}{2}\cos(2\omega_1 t + \theta_1) = \frac{A_1 A_2}{2}\cos\theta_1 \quad (14)$$

B. Fast Fourier Transforms (FFT)

An analytical model for calculating RF beat frequencies was proposed by Stelmakh et al [7], corresponding to the heterodyne spatial resolution between two lateral modes of order p and p', belonging to the same longitudinal mode m. Fig. 7 shows a beat note achieved for a specific input current at a transversal coordinate x. Equation (15) corresponds to the beat frequencies $\omega_{pp'}$ according to [7], for the spectral line λ_o. W is the laser cavity width, c is the light speed and n_{ph} corresponds to the refraction index related with the semiconductor material active layer. Fig. 7 shows a FFT sample from the photodetector signal for a specific transverse mode. The pumping current applied to the diode is I_F= 490 mA and the beat frequency is approx. 1.4 GHz corresponding to the overlap of modes TEM_{00} and TEM_{10}.

$$\omega_{pp'} = \omega_{mp'} - \omega_{mp} = \frac{\pi c \lambda_o}{4 n_{ph}^2(\lambda_o)W^2}(p'^2 - p^2) \quad (15)$$
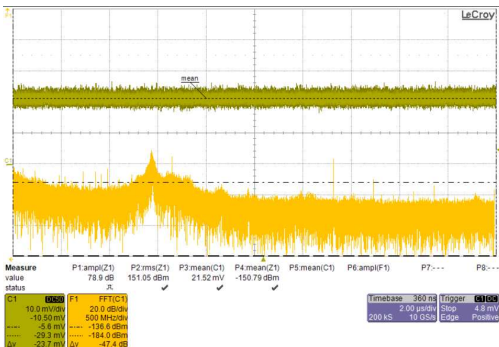

Fig 7. FFT sample on a specific transversal coordinate x using the set-up of Fig 8. Channel C1 (upper trace) means the photo-sensor signal while F1 channel (bottom trace) demonstrates the FFT calculation for C1.

IV. EXPERIMENTAL SET-UP

The optical system shown in Fig 8 was developed and employed for supporting the FFT extractions. The laser beam was focused precisely on the active area of the fast photodetector. Initially, by using spherical lenses and neutral density filters. Later, it was remarkably improved with the use of cylindrical lenses. The normalized output of the photodetector was connected to a spectrum analyzer with a high sampling rate, 5 GS/s, with signal post-processing capability to execute fast Fourier transform (FFT) routines. The BALD had its temperature case controlled and kept at 20 °C, and its pumping current was fully stabilized by a proper controller and free from spurious current and ripples.
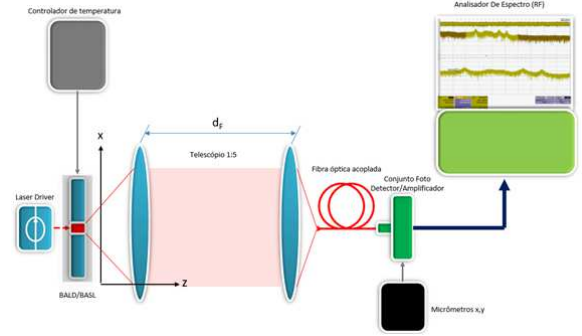

Fig. 8. Proposed test bed diagram for the experimental data collections, necessary for measuring the beat frequency positions in respect to their x coordinates. Spherical lenses was applied in companion with a 100 μm optical fiber for an initial qualification measure check.

As demonstrated by [8], the optical system received a correction with the implementation of cylindrical lenses. Fig. 9 shows, as per example, the effect of the double intensity peaks, corrected by the cylindrical optical part.
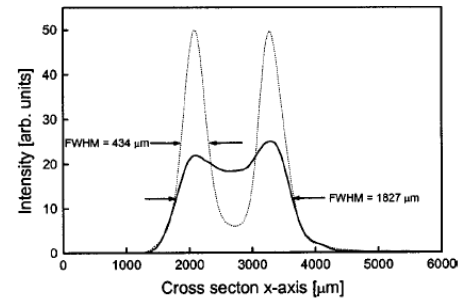

Fig. 9 Intensity peaks observed in the far-field region for the laser beam (solid curve) using spherical optics and the same signal measured by the new optical set-up (dashed curve)[8].

With the new optical set-up, it was possible to use a larger, 400 μm diameter optical fiber optic that increased also the overall sensitivity of the whole set-up.

V. RESULTS

Shown in Fig. 10 is an example of several beat frequencies extracted at high pump current.
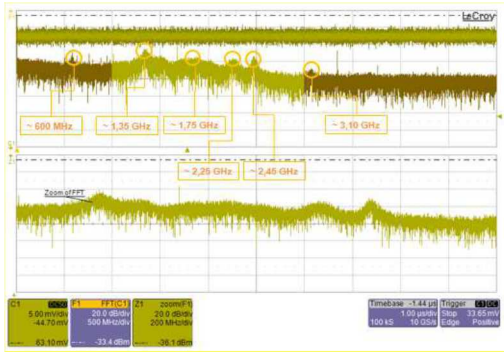
Fig. 10 FFT sample with identification of the transversal mode beat frequencies.

For comparison purposes, in reference to the work of [7], the measured beat frequencies between two lateral modes for a given group of longitudinal modes m are shown in table 1 as a function of pump current. Some beat frequencies show little variation with direct current I_F in the diode, others a little bit more. The beat frequencies' positions have been recorded by a precise micrometer mechanism that sweeps the transversal axis and are shown in Fig. 11.

TABLE I.   MEASURED BEAT FREQUENCIES, SPHERICAL LENSES

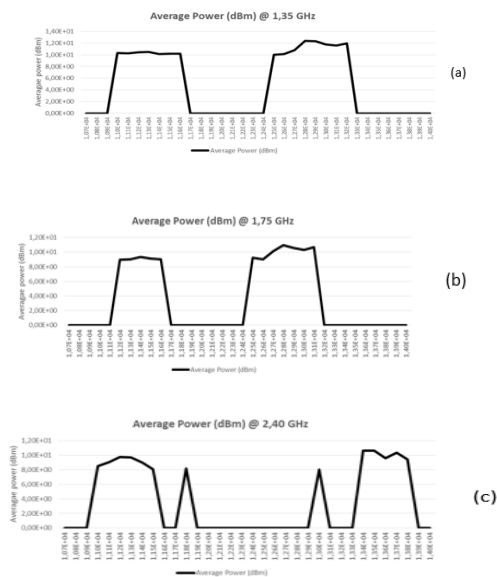| I_F (mA)	Distribution of frequency beats according to maximum FFT amplitudes (GHz)					
	$f_{pp'1}$	$f_{pp'2}$	$f_{pp'3}$	$f_{pp'4}$	$f_{pp'5}$	$f_{pp'6}$
300						
320			1,75	1,90		
340			1,70	1,95		
360		1,25	1,75	2,25	2,65	
380		1,28	1,75	1,90	2,10	
400		1,31	1,75	1,93	2,30	
420		1,35	1,75	2,20	2,32	
440		1,30	1,75		2,38	
460		1,35	1,82	2,25	2,39	
480		1,40	1,80	2,20	2,40	
500		1,35	1,75	2,25	2,45	3,10
520		1,35	1,75	2,25	2,60	3,10
540		1,35		2,25	2,60	3,10
560		1,35	2,25		2,60	
580		1,35	2,30		2,65	

(a)

(b)

(c)

Fig. 11 a, b, c. Measurement average values for FFT amplitudes (beat signals) as a function of spatially resolved transverse position for the first transverse TEM modes: (a) 1,35 GHz, (b) 1,75 GHz e (c) 2,40 GHz. X-axis is the position in meters.

As can be seen in Fig. 11, the lateral displacement along the x-axis of the modal distribution, is symmetrical for all frequencies as expected in [7]. However, we observed a loss in position resolution that would allow us to unequivocally determine which modes participate in each beat frequency. This has been now resolved with the new optical set-up using cylindrical lenses.

VI. CONCLUSIONS

The innovation, carried out by this work, refers to the use of the oscillation threshold condition for the lateral modes using rate equations according to the work of [1]. As a second innovative aspect, an experimental method for reading the TEM beats was developed to identify the position of the modes. Up to the present moment, we have measured the beat frequencies (table 1) at 1.35 GHz, 1,75 GHz and 2,40 GHz, which most likely correspond to the beating of the TEM_{00} with TEM_{10}, TEM_{10} with TEM_{20} and TEM_{20} with TEM_{30}, according to the findings of [7]. We observed a lack of resolution for the beat frequency positions, a task we expect to improve in the next step using a newer configuration to the experimental arrangement with the usage of purely cylindrical optics. In this first stage, the software tool presented a good relationship with a typical single stripe semiconductor laser response, observed in many simulations' tasks, as shown by figure 11. Especially, the order at which new modes enter oscillation as a function of pump current seems to agree well. In the next part of this work, we will analyze the agreement between the simulation model, according to Fig.3, with the oscillation thresholds effectively observed using the new optical set-up and as shown in the Fig. 3 and table 1. While the testing method based on heterodyning has been shown before, it is to our knowledge the first time that a numerical simulation is demonstrated based on rate equations.

REFERENCES

[1] K. Kubodera, and K. Otsuka, "Single-transverse-mode slab waveguide laser", Journal of Applied Physics 50(2), February 1979.
[2] D. Lenstra and M. Yousefi, "Rate-equation model for multi-mode semiconductor lasers with spatial hole burning," Optics Express, 22(7),8143-8149, January 2014.
[3] K. Ebeling, R. Michalzik and P. Unger, "Numerical simulation of broad area high power semiconductor laser amplifiers," IEEE Journal of Quantum Electronics, Vol 33, No.12 , December 1997.
[4] P. Agrawal, and J. Marciante, "Spatio-temporal characteristics of filamentation in broad area semiconductor lasers", IEEE Journal of Quantum Electronics, Vol 33, No.07 , July 1997.
[5] A. Zeghuzi, M. Radziunas, H. Wenzel, H. Wünsche, U. Bandelow and A. Knigge, " Modeling of current spreading in high-power broad-area lasers and its impact on the lateral far field divergence," Procedures of SPIE Vol. 10526, 105261H, February 2018.
[6] T. Paoli, "Waveguiding in a stripe-geometry junction laser," IEEE Journal Of Quantum Electronics, Vol QE-13, No.08 , August 1977.
[7] N. Stelmakh and M. Vasilyev, "Spatially-resolved self-heterodyne spectroscopy of lateral modes of broad-area laser diodes" – Optical Society of America, vol. 22, No. 4, February 2014.
[8] C. Mingjun, N. Bogh, B. Thestrup and P. Petersen, "Improvement of the beam quality of a broad-area diode laser using double feedback from two external mirrors", Applied Physics Letters, Vol 85, No 07, August 2004.